Eur Biophys J (1998) 27: 532–539

ARTICLE

Dean C. Bottino · Lisa J. Fauci

A computational model of ameboid deformation and locomotion

Received: 5 January 1998 / Revised version: 23 March 1998 / Accepted: 26 March 1998

Abstract Traditional continuum models of ameboid deformation and locomotion are limited by the computational difficulties intrinsic in free boundary conditions. A new model using the immersed boundary method overcomes these difficulties by representing the cell as a force field immersed in fluid domain. The forces can be derived from a direct mechanical interpretation of such cell components as the cell membrane, the actin cortex, and the transmembrane adhesions between the cytoskeleton and the substratum. The numerical cytoskeleton, modeled as a dynamic network of immersed springs, is able to qualitatively model the passive mechanical behavior of a shear-thinning viscoelastic fluid (Bottino 1997). The same network is used to generate active protrusive and contractile forces. When coordinated with the attachment-detachment cycle of the cell's adhesions to the substratum, these forces produce directed locomotion of the model ameba. With this model it is possible to study the effects of altering the numerical parameters upon the motility of the model cell in a manner suggestive of genetic deletion experiments. In the context of this ameboid cell model and its numerical implementation, simulations involving multicellular interaction, detailed internal signaling, and complex substrate geometries are tractable.

Key words Ameboid deformation · Ameboid locomotion · Computational model

1 Introduction

The basic mechanisms generating ameboid locomotion and deformation are recognized to be highly conserved across species and are therefore relevant in several branches of biology. For example, the human body's immune system depends upon the chemotactic and phagocytotic behavior of crawling white blood cells to remove dead cell material and antigen-antibody complexes from tissue. During embryonic development, nerve growth cones, guided by contact with growth-promoting and growth-inhibiting regions in the extracellular matrix, "crawl" and thereby extend axons throughout the forming organism. Sarcoma cells, possessing the mechanisms for generating ameboid locomotion but lacking the regulatory mechanisms of healthy cells, augment their invasion of healthy tissue by active crawling. In a phenomenon suggestive of embryonic development, genetically identical starving slime-mold amebas are able to specialize and aggregate into multicellular crawling slugs. A versatile mechanical model of an ameboid cell can aid in understanding the relative importance of the proposed force-generating mechanisms responsible for these motions. Such a model can also be adapted to simulate more complex intercellular signaling and the resultant multicellular interactions.

The immersed boundary method has been used in such moving-boundary biofluiddynamical models as the human heart (Peskin 1977; Peskin and McQueen 1989a; Peskin and McQueen 1989b), flagellated microorganisms (Fauci and Peskin 1988; Fauci 1990; Fauci 1993; Fauci and McDonald 1995; Dillon, Fauci, and Gaver 1995), and the aggregation of blood platelets (Fogelson and Fauci 1993). This method overcomes typical computational obstacles related to free boundaries by modeling the boundaries as force fields immersed in a larger, simpler computational domain. Therefore, this method is well-suited for modelling shape changes in ameboid cells. In this paper we explore the ways in which the immersed boundary method can be implemented in order to model passive cytoskeletal behavior, active deformation, and the coordination of protrusion, retraction, and adhesion into directed movement.

In Section 2, we propose a two-dimensional mechanical model of the cell in the context of the immersed boundary method. We represent the cell membrane as an im-

D. C. Bottino
Department of Mathematics, University of Utah,
Salt Lake City, UT 84112, USA
e-mail: bottino@math.utah.edu

L. J. Fauci
Department of Mathematics, Tulane University,
New Orleans, LA 70118, USA

permeable immersed boundary. The actin cytoskeleton is modeled as a network of points linked by elastic elements. The points are located both in the interior of the cell and on the cell membrane. The target length and stiffness of an elastic link joining any two actin points varies as a function of distance, local chemoattractant and internal signal concentrations, and time. In addition to providing passive mechanical strength, this dynamic actin network generates the active forces in the model cell. The substratum consists of a rigid linear boundary beneath the model cell. The transmembrane adhesions are modeled as links between the membrane-embedded actin points and the substratum.

We present results of ameboid locomotion simulations in Section 3. Two protrusion models are simulated: the actin polymerization model and the ectoplasmic contraction model. A third model cell similar to the actin polymerization model but with impaired contractile ability is also devised. The motility of the three model cells is compared.

1.1 Biological background

The dynamics of the actin cytoskeleton are essential for ameboid locomotion.Viscometer tests indicate that actin gel is a shear-thinning thixotropic viscoelastic fluid. It is believed that under stress, "islands" of crosslinked actin are broken apart and flow freely past each other, but when allowed to rest these islands form elastic interconnections due to actin polymerization and crosslinking (Janmey 1991; Sackmann 1994). There are three major proposed mechanisms for the generation of protrusive force in ameboid cells, all of which require actin polymerization and depolymerization. Actin **polymerization** is known to occur at the leading edge of advancing cells (Fukui 1993) and produces sufficient force to deform the membranes of fluid-filled vesicles (Cortese et al. 1989). The **contraction** of actomyosin fibers in *Ameba proteus* is thought to generate sufficient hydrostatic force for the flow into — and consequently the protrusion of — areas of the cell cortex where the cytoskeleton has been weakened (Alberts et al. 1994). Disruption, or "solation", of actin gel can cause the osmotic flow of cytosol, resulting in **swelling** of the solated region, and therefore protrusion (Oster and Perelson 1985).

The cell membrane has a mechanically passive role in cell motion. Ameboid cells have more than twice the membrane area needed to enclose their volumes in a sphere (Chien et al. 1984); thus the membrane "unfolds" in order to permit the protrusion of pseudopodia. The membrane is also important for the conversion of external chemotactic gradients into internal signals via membrane-bound receptors (Devreotes and Zigmond 1988). Transmembrane adhesion proteins provide mechanical connections between the cytoskeleton and the extracellular medium, and there is evidence that in *Dictyostelium* the level of adhesion varies periodically in order to facilitate motion (Schindl et al. 1995). These adhesions are essential for ameboid locomotion on a two-dimensional substrate (Lackie and Wilkinson 1984).

2 The model

We restrict our attention to the two-dimensional section of the ameba parallel to the cell's direction of motion and perpendicular to the substratum. This is the projection from three to two dimensions which captures the essential aspects of cell locomotion.

2.1 Continuum description of the cell

The ameboid cell and the substratum on which it crawls are modeled as neutrally buoyant structures immersed in a square fluid domain $\Omega = [0, L] \times [0, L] \subset \mathbf{R}^2$. The model cell consists of the membrane $\mathbf{M}(s, t)$, the fluid bounded by the membrane, the actin network $\mathbf{A}_j(t)$, and the focal attachments $\mathbf{H}_k(t)$, which link the actin network to the substratum $\mathbf{W}(s, t)$.

2.1.1 Governing equations

The fluid motion is described by the incompressible Navier-Stokes equations, given by

$$\rho\left(\frac{\partial \mathbf{u}}{\partial t} + \mathbf{u}\cdot\nabla\mathbf{u}\right) = -\nabla p + \mu\Delta\mathbf{u} + \mathbf{F}, \tag{1}$$

$$\nabla\cdot\mathbf{u} = 0 \tag{2}$$

in Ω, with periodic boundary conditions on Ω. Equation (1) is Newton's Second Law, where ρ is the fluid density, μ is the viscosity, $\mathbf{u}$ is the fluid velocity, p is the hydrodynamic pressure, and $\mathbf{F}$ is the force of the immersed structures on the fluid. Equation (2) is the conservation of mass equation for incompressible flow.

The immersed structures $\mathbf{W}(s, t)$, $\mathbf{M}(s, t)$, $\mathbf{A}_j(t)$, and $\mathbf{H}_k(t)$ move at the local fluid velocity. We express this as

$$\frac{d}{dt}\mathbf{X} = \mathbf{u}(\mathbf{X}, t) \tag{3}$$

for $\mathbf{X} \in \{\mathbf{W}, \mathbf{M}, \mathbf{A}, \mathbf{H}\}$. As a structure moves with the fluid, it is strained from its original configuration, and in some cases its resting or target configuration varies as a function of time and chemoattractant/signal concentration. This strain $e_X(s, t)$ from the target configuration of structure $\mathbf{X}$ results in the formation of tension $T_X(s, t) = T(e_X(s, t))$ in the structure. This internal tension is manifested as a force density distribution $\mathbf{f}_X(s, t)$ supported all along $\{\mathbf{X}(s, t)|s\}$. Since the mass of these neutrally buoyant structures is inherited from the ambient fluid, these internal forces are transmitted directly to the surrounding fluid via

$$\mathbf{F}_X(x,t) = \int_{I_X} \mathbf{f}_X(s,t)\,\delta\big(\mathbf{X}(s,t) - \mathbf{x}\big)\,ds \tag{4}$$

for $\mathbf{X} \in \{\mathbf{M}, \mathbf{W}\}$. Here δ is the two-dimensional Dirac delta function and I_X is the set parameterizing $\mathbf{X}$. The force-spreading integral for the actin network, derived in (Bot-

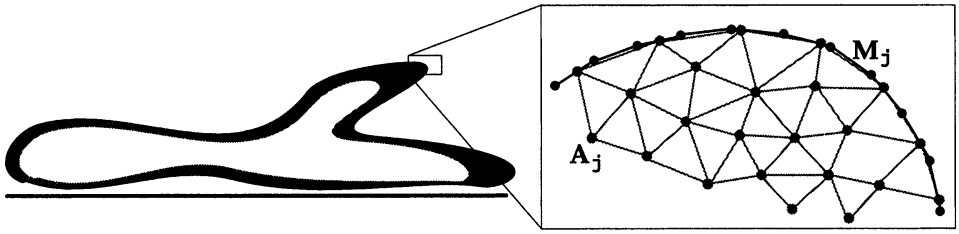

Fig. 1 Schematic of cellular components in model. Note that a subset of the actin nodes $\mathbf{A}_j$ are embedded in the curve defined by the membrane points $\mathbf{M}_j$, allowing transmission of force from the model cytoskeleton to the model membrane. The entanglements among actin nodes are modeled as linear springs that form if the nodes are sufficiently close and break under excessive strain

tino 1996; Bottino 1997), is similar to (4). The net force of the immersed structures on the fluid is given by

$$\mathbf{F} = \mathbf{F}_W + \mathbf{F}_M + \mathbf{F}_A + \mathbf{F}_H. \tag{5}$$

This total force $\mathbf{F}$ enters as the force term in (1), and we thus obtain mutual coupling between the fluid motion and the immersed structures. This general method and its numerical implementation, originally introduced by Peskin in (Peskin 1977), are together referred to as the immersed boundary method.

2.1.2 Immersed structures and forcing among them

The essential aspects of the model are contained in the representation of the immersed structures and the forces they exert on themselves and on each other.

Substratum. The substratum, or "wall", is parameterized by $\mathbf{W}(s, t)$ for $s \in [0, L]$ and is given initially by $\mathbf{W}(s, 0) = (s, y_w)$. The wall is modeled as an inextensible impermeable boundary. Its rigidity is maintained by tethering the wall to a fixed position in space and applying penalty forces to restore the wall should it deviate from its original position.

Membrane. The cell membrane is modeled as the loop parameterized by $\mathbf{M}(s, t)$ for $s \in [0, 2\pi r_c]$, where r_c is the initial cell radius. The local strain $e(s)$ of the membrane is given by $e(s) = \|\partial\mathbf{M}/\partial s\| - 1$. An initial approximation for the tension $T(e)$ in the membrane would be a hookean relationship with stiffness S_M: $T = S_M e$. Ameboid cells, however, have up to 137% excess membrane area; as a result, the membrane unfolds with little or no resistance up to its maximum area, at which point it strongly resists further increases in area (Chien et al. 1984). If we think of the length of $\mathbf{M}(s, t)$ in our two-dimensional model as the "effective area" of the membrane, folding included, we would like $\{\mathbf{M}(s, t)\}$ to stretch easily up to, say, twice its original length (corresponding locally to $e(s) = 1$) before becoming strongly inextensible. For this reason we use a tension function T of the form

$$T = eS_M 10^{e^\sigma}, \tag{6}$$

where σ is a positive odd integer.[1] Note that increasing σ increases the strain threshold above which membrane tension becomes appreciable. Given the tension $T(s)$ and the unit tangent vector $\tau(s)$ along the membrane $\mathbf{M}(s, t)$, the force density (Peskin and McQueen 1989a) is given by

$$\mathbf{f}_M = \frac{\partial}{\partial s}(T\tau). \tag{7}$$

Actin cytoskeleton. The actin network is modeled as a discrete collection of nodes $\mathbf{A}_j(t)$ (representing "islands" of crosslinked **F**-actin described in Janmey (1991)) joined by spring-like links or fibers. Initially, $\mathbf{A}_1, \ldots, \mathbf{A}_{N_{AM}}$ are distributed evently along the membrane and are referred to as the "actin-membrane anchors" and $\mathbf{A}_{N_{AM}+1}, \ldots, \mathbf{A}_{N_A}$ are distributed in the cell interior as a hexagonal array with separation distance δA. Figure 1 shows the configuration of the membrane, actin, and substratum.

The actin-myosin entanglements among the actin "islands" are modeled as links among the points $\mathbf{A}_i$. The tension on a link from $\mathbf{A}_i$ to $\mathbf{A}_j$ is assumed to be a linear function of the strain:

$$T_{ij} = S_{ij}\left(\frac{\|\mathbf{A}_i - \mathbf{A}_j\|}{\delta\mathbf{A}_{ij}} - 1\right), \tag{8}$$

where S_{ij} and δA_{ij} are sparse symmetric matrices of stiffness constants and resting lengths, respectively, and $S_{ij} = 0$ means that there is no link between the nodes $\mathbf{A}_i$ and $\mathbf{A}_j$. The force density at each point is then

$$\mathbf{f}_i = \frac{1}{\delta A}\sum_j T_{ij}\frac{\mathbf{A}_i - \mathbf{A}_j}{\|\mathbf{A}_i - \mathbf{A}_j\|}. \tag{9}$$

The dependence of S_{ij} and δA_{ij} on time, chemoattactant/signal concentration, and strain comprises the fundamental mechanism for deformation and locomotion in the model.

The linear force-extension relation of the model entanglements given in (8) can readily be replaced by nonlinear force-extension relations such as those derived for wormlike chains (Kroy and Frey 1996). The force scaling in (9) is chosen to maintain consistent mechanical properties of the network as numerical resolution is increased, that is, as $\delta A \to 0$. The definition of the network model was based

[1] The functional form of (6) was chosen arbitrarily because it had the desired property of a rapid transition from weak compression to strong tension. Although it may be possible to use statistical mechanics to derive from first principles a stress-strain relationship for a folded membrane, such an improvement would not be likely to have a significant impact on these simulations

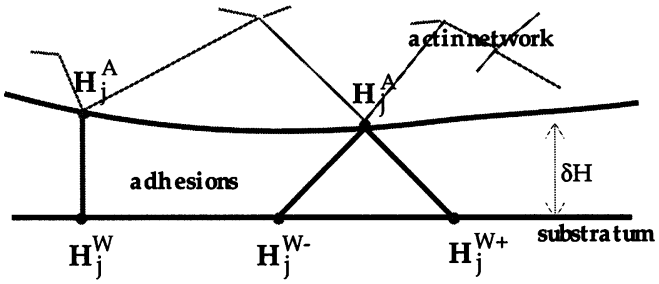

Fig. 2 Schematic of transmembrane tethers to the substrate in model. A pair of elastic links from the substrate to a membrane-embedded actin node prevents the node from slipping horizontally. The resting distance of the cell from the substrate is a nonzero numerical parameter $\delta H \sim \Delta x$, where Δx is the finite difference fluid mesh width, in order to allow the cell to move relative to the substrate. Note that as $\Delta x \to 0$, $\delta H \to 0$

upon the analogy between the nodes $\mathbf{A}_j$ and the centers of crosslinked actin islands described by Janmey and others (Janmey 1991; Tempel et al. 1996). This analogy is less useful if the spacing δA between model actin nodes varies significantly from the average length of the inter-island entanglements in the "microgel phase" discussed by Sackmann (1994).

The passive mechanical behavior of this network can be determined by the linking rules among the actin nodes. For example, suppose two points $\mathbf{A}_i$ and $\mathbf{A}_j$ are joined by a link with constant stiffness $S_{ij} = S_A$ and constant resting length $\delta A_{ij} = \delta_A$ whenever $\mathbf{A}_j$ is within the annular "capture region" centered at $\mathbf{A}_i$, that is, whenever $d_{min} < ||\mathbf{A}_i - \mathbf{A}_j|| < d_{max}$. It has been shown in numerical tests that such a network behaves mechanically like a shear-thinning viscoelastic fluid (Bottino 1997). Appropriate choice of stiffness constants S_{ij} and resting lengths δA_{ij} as functions of chemoattractant concentration, internal signal concentration, and time also allow us to model *active* cytoskeletal protrusion and contraction. These functions either replace or augment one of the above mentioned passive forcing rules.

The attachments of the model cell to the substrate are modeled as elastic links from membrane-embedded actin nodes to points embedded in the substrate. While the leading edge of the model cell is protruding forward, attachments in the rear of the cell prevent the cell from slipping backwards. Before the newly formed protrusion is pulled back toward the cell body, attachments are established from the protrusion to the substratum and released in the rear of the cell, so that the frontal contraction will cause the model cell to pull itself forward (Fig. 2).

2.2 Discrete system and numerical scheme

In order to solve the equations in Section 2.1 numerically we discretize them both spatially and temporally. The fluid domain $\Omega = [0, L] \times [0, L]$ is represented by an $N_G \times N_G$ finite difference grid. The periodicity of Ω implies that 0 and N_G index the same points. At time $t = n\Delta t$ the immersed boundaries $\mathbf{W}(s, t)$ and $\mathbf{M}(s, t)$ are represented as discrete collections of points $\{\mathbf{W}_i^n\}_{i=1}^{N_W}$ and $\{\mathbf{M}_i^n\}_{i=1}^{N_M}$, while the immersed structures $\mathbf{A}(s, t) = \{\mathbf{A}_i^n\}_{i=1}^{N_A}$ and $\mathbf{H}(s, t) = \{\mathbf{H}_j^A, \mathbf{H}_j^W\}_{i=1}^{N_A}$ are already discretized. The general rule for discretization of the parameterizations is $\mathbf{X}_i^n = \mathbf{X}(i\Delta s, n\Delta t)$, where Δs is a structure-specific numerical parameter.

We use the following finite difference discretization of the incompressible Navier-Stokes equations (1) and (2):

$$\rho\left(\frac{\mathbf{u}^{n+1} - \mathbf{u}^n}{\Delta t} + \sum_{s=1}^{\eta} u_s^n D_s^{\pm} \mathbf{u}^n\right) =$$

$$-\mathbf{D}^0 p^{n+1} + \mu \sum_{s=1}^{\eta} D_s^+ D_s^- \mathbf{u}^{n+1} + \mathbf{F}^n, \tag{10}$$

$$\mathbf{D}^0 \cdot \mathbf{u}^{n+1} = 0, \tag{11}$$

where D^+ is the forward difference operator, D^- is backward difference, $\mathbf{D}^0$ is center difference, $\mathbf{D}^0\cdot$ denotes discrete center difference divergence, $D_s^{\pm}$ is upwind difference (if $\sigma = \text{sign}(u_s)$ then $D_s^{\pm} \equiv D_s^{-\sigma}$), and η is the number of dimensions, in our case two.

Given $\mathbf{u}^n$ and $\{\mathbf{X}_i^n\}$, a single timestep of this simulation proceeds as follows:

1. The immersed points $\{\mathbf{X}_i^n\}$ are moved according to the interpolated local fluid velocity to compute $\{\mathbf{X}_i^{n+1}\}$.
2. The resulting strain on the links between the points is measured, and penalty forces $\mathbf{f}_i$ are assigned to all of the points.
3. The forces on the points are spread back onto the fluid grid and appear as the $\mathbf{F}^n$ term in (10).
4. The discretized Navier -Stokes equations (10) are solved by the fast-fourier transform method given in (Peskin and McQueen) to obtain $\mathbf{u}^{n+1}$.

A more detailed explanation of the numerical implementation of this scheme can be found in (Bottino 1997; Bottino 1996).

3 Numerical results

3.1 Wall shear experiments

The passive mechanical behavior of the numerical network defined in the previous section has been studied extensively in (Bottino 1997; Bottino 1996). The response of the network to shear stress is measured by constructing a numerical apparatus consisting of model network sandwiched between a fixed wall and a wall which is subject to a horizontal shearing force (Fig. 3). The deformation of the model network as a function of time (the "strain history") was recorded and linear viscoelastic models were fit to the data. It was determined that the mechanical behavior of the capture annulus network was well-characterized by a linear viscoelastic fluid model, and that the effective viscosity of the network diminished with increasing shear stress. Similar mechanical behavior has also been observed

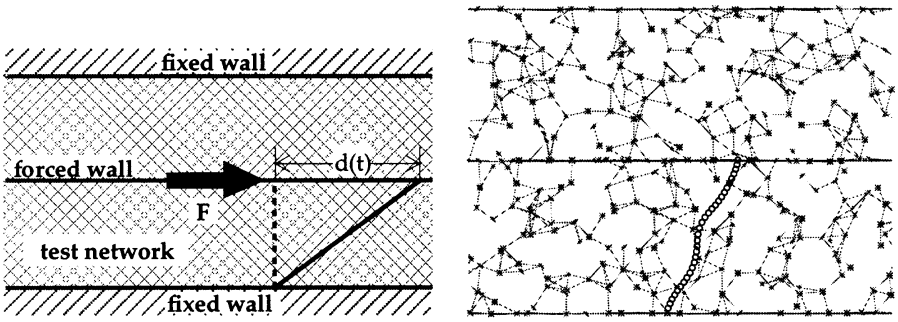

Fig. 3 A schematic of numerical wall-shear apparatus (*left*) and snapshot of annulus network under shear (*right*). A horizontal force is applied along the center partition (the "forced wall") in the indicated direction, and the deformation of the numerical network is measured as a function of time. The circular marker points in the right figure were vertical before the force was applied

in the cytoskeleton of ameboid cells (Evans 1984; Waugh and Tsai 1994). The same wall-shear experiments were used in (Bottino 1996) to show the convergence of the numerical network under the force scaling rules described in section 2.1.2.

3.2 Micropipette aspiration

Numerical simulations modeled after *in vivo* micropipette aspiration experiments (Waugh and Tsai 1994; Evans 1984; Chien et al. 1984) may reveal the aggregate mechanical properties of the model cell as well as the individual properties of the cell membrane and the actin cytoskeleton under various linking and forcing rules. There are several advantages to simulating such biological experiments rather than moving directly to modeling ameboid locomotion. First of all the biological experiments provide better-defined quantitative and qualitative information to which the numerical results can be compared. Secondly, the numerical experiments provide an environment in which it is easier to measure the effects of numerical parameters on the passive mechanical behavior of individual cell components as well as the effects of these components on the entire model cell. An example of one of the micropipette aspiration simulations performed in (Bottino 1997) is shown in Fig. 4.

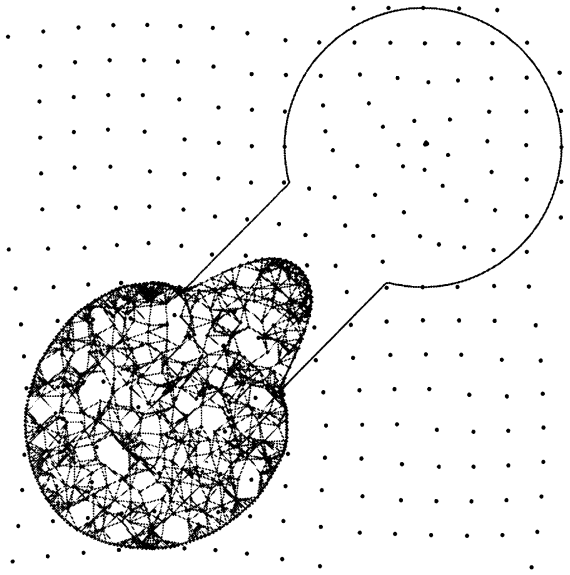

Fig. 4 Numerical micropipette aspiration of model cell. A negative pressure is established inside the numerical pipette and bulb apparatus by imposing a "sink" (in which $\nabla \cdot \mathbf{u} < 0$) in the center of the bulb and a line of sources ($\nabla \cdot \mathbf{u} > 0$) exterior to the model cell and apparatus. The model cell is shown partially aspired into the apparatus after four seconds of simulated time

3.3 Ameboid locomotion

Two of the proposed mechanisms of locomotion described in Section 1.1 were simulated: the **actin polymerization model** and the **ectoplasmic (tube) contraction model**. Both models were computed using a 64×64 square fluid grid of length $L = 0.0025$ cm with a cell of initial radius $r_c = L/8 = 3\ \mu m$, which is approximately the size of a human neutrophil (Alberts et al. 1994).

Both model cells move by undergoing an extension-retraction cycle of periodic $\omega = 30$ sec, which is approximately the period of the Ca^{++} oscillations observed in translocating neutrophils (Bray 1992). The model cell is partitioned, or "polarized", into posterior and anterior portions based on ambient chemoattractant concentration. During the extension phase, the model cell's posterior focal adhesions are made to attach statically to the substratum while the anterior adhesions are allowed to slide freely. During the retraction phase, the cell's anterior substratum adhesions are anchored and the posterior adhesions are allowed to slide. The joint action of the contraction and the anterior adhesions result in forward motion.

Both model cells also include a mechanism for modeling squeezing of the cell due to actomyosin contraction, referred to hereafter as "ectoplasmic contraction". The squeezing is modeled as the establishment of tensile transcellular links orthogonal to the chemoattractant gradient. Transcellular links are necessary to produce a global contraction of the model cell in two dimenisons.

Microbiologists often use genetic deletions to disable part of an ameboid cell's molecular apparatus in order to observe the effects of the absence or alteration of that mechanism on the cell's motility. Similarly, we can modify or eliminate certain numerical parameters and compare the motility behavior of this "mutant" model cell to the "wild-type" standard cell. As our confidence in this model

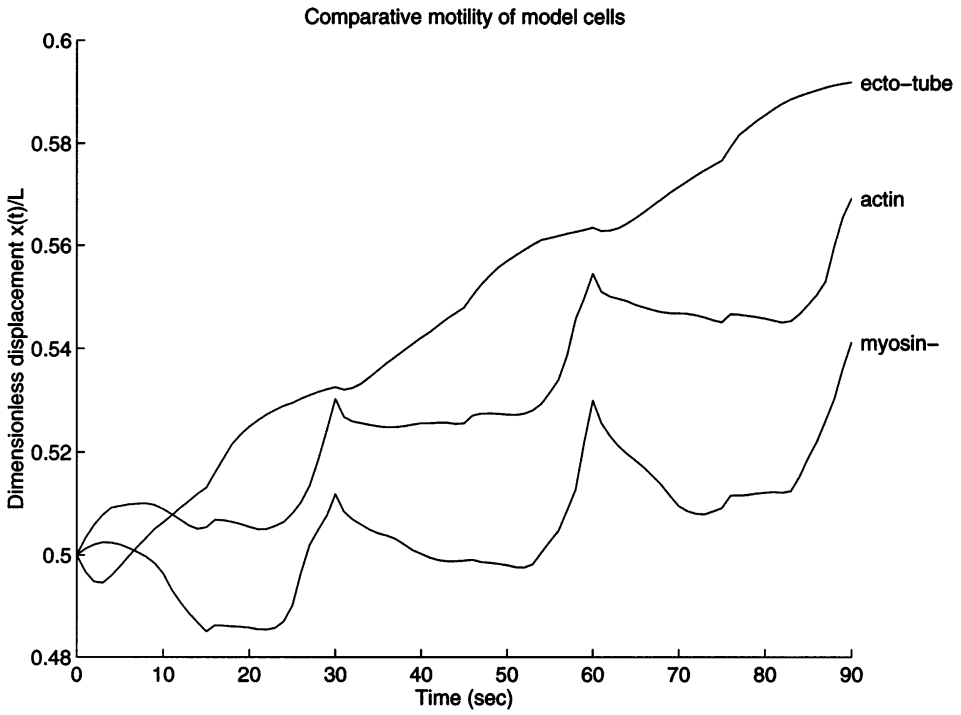

Fig. 5 Motility comparison of actin polymerization, ectoplasmic contraction, and myosin$^-$ model cells. The x-component $x(t)$ of the center of mass of each model shell is shown, scaled by the length $L = 0.0025$ cm of the domain. Thus by the end of three cycles, the ectoplasmic contraction model cell has translocated by 9% of the length of the domain, or approximately 2.25 μm. The numerical cells' average translocation velocities of approximately 1.5 μm/min are slower by a factor of 10 than the velocities observed in living (three-dimensional) neutrophils

increases we may use such studies to predict the results of actual genetic deletion experiments. As an example, we devised an additional model cell in which the transcellular ectoplasmic contraction-generating links were turned off. The role of these links is analogous to the role of sliding filaments of actin and myosin-II in *Dictystelium discoideum* that are believed to generate the ectoplasmic contraction discussed previously. In biology, similar mutants have been genetically engineered by recombining an incomplete myosin-II gene into the target cell's DNA. Such cells are rounder and less polar than normal cells, and they move at an average rate of translocation less than half that of normal cells (Wessels et al. 1988).

The following three model cells were tested:

– In the **actin polymerization** model cell, the cell maintains its flattened shape by way of a continual "ectoplasmic contraction". During the extension phase of motion, links with temporally increasing resting lengths form in the anterior portion of the cell, causing the cell to protrude in the forward direction. During the retraction phase, reduction of resting lengths causes an active contraction of those same links in the anterior portion of the cell.
– In the **ectoplasmic contraction** model cell, transcellular squeezing links are also used, but the links vary in resting length and in strength sinusoidally in time. During the extension phase the squeezing links are at their maximum stiffness and contractility. Simultaneously, the actin links ℓ_{ij} in the anterior part of the cell are disrupted by setting $S_{ij} = 0$, allowing the fluid inside the model cell to flow into the weakened region. During the retraction phase, the squeezing links are weakened while the stiffness of the distended links in the anterior region of the cell is restored, resulting in a longitudinal contraction of the model cell. Note that the transcellular contraction is homogenous in space for all time; it is the differential adhesion and "solation" of anterior network links that results in directed motion.
– The **myosin**$^-$ model cell is identical to the actin polymerization cell, but the transcellular squeezing links have been disabled.

3.3.1 Comparison of model cells

Both the actin polymerization and the ectoplasmic contraction model simulations were able to generate translocation of the model cell. Figure 6 shows successive snapshots of the configurations of the actin polymerization, ectoplasmic contraction, and myosin$^-$ model cells, taken at regular intervals over the 3-cycle, 90-second span of the simulation. At regular time intervals the center of mass of the model ameba is computed, allowing us to compare the histories of the distance traveled, and therefore the average velocities, for the model cells. Figure 5 compares the motility of the model cells over the three movement cycles.

In the third column of Fig. 6 and in Fig. 5, we see the effect of the lack of squeezing on the myosin$^-$ model cell. The motility of the squeezing-deficient model cell is noticeably impaired, but in steady state the average velocity of this cell is only slightly less than that of the standard cells. Note that the initial configuration of the cell was the same as that for the other cells; in a sense we have modeled a cell which flattens like the standard cell but once it starts moving it is no longer capable of generating actomyosin contractions, which causes the cell to lose its flattened shape as the simulation progresses.

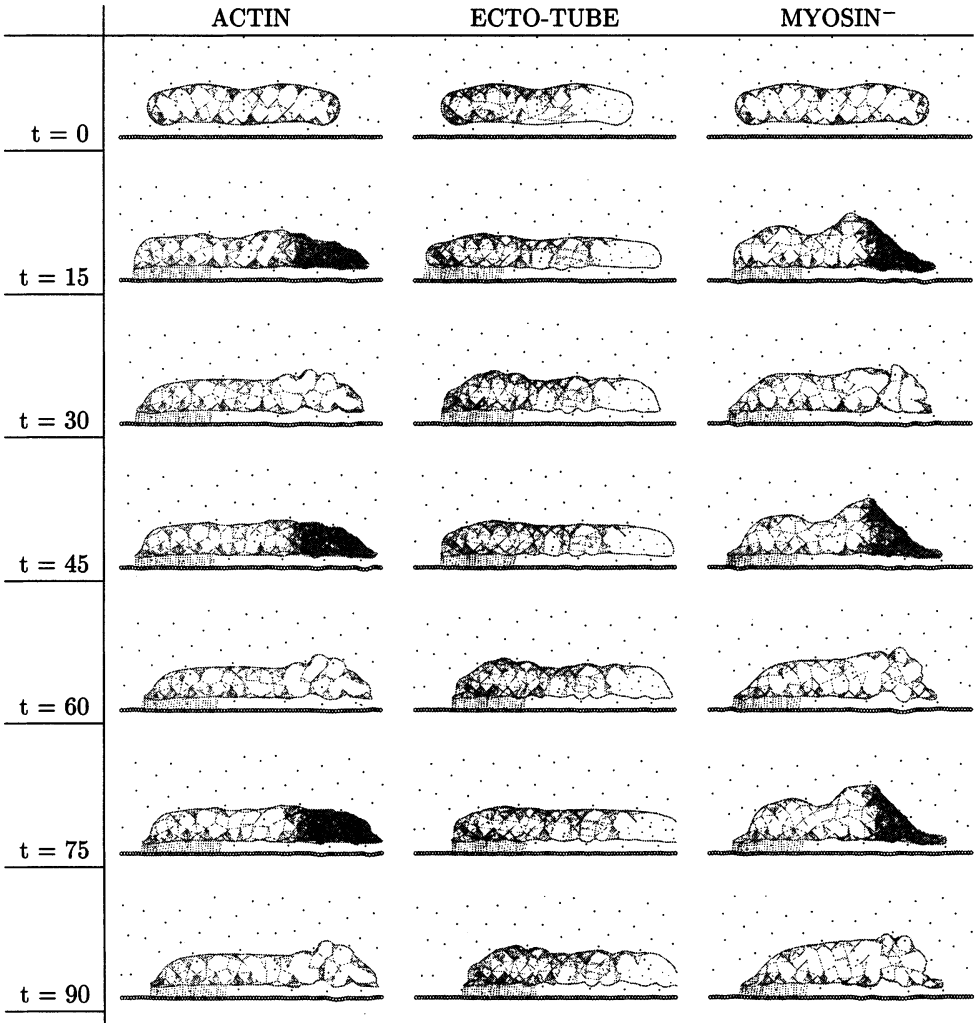

Fig. 6 Comparison of actin polymerization, ectoplasmic "tube" contraction and myosin$^-$ model cells. The model cells are shown undergoing three 30-second extension/retraction cycles. The areas of the network with a greater density of elastic links result in the darker appearance of the protruding pseudopodia in the actin and myosin$^-$ model cells. The links extending from the model cell to the substrate indicate which adhesions are currently active. The snapshots for t = 30, 60, 90 show the instant *after* the model adhesions were switched from the anterior to the posterior portion of the cell following pseudopodial retraction

4 Discussion

The model and numerical method presented in this paper comprise a promising starting point for the study of ameboid deformation and locomotion. The numerical experiments involving alteration of the transcellular squeezing stiffness in the model cells give an example of how the model can be used as a testbed for comparing the relative importance of various mechanical properties of an ameboid cell to its locomotion. Other parameters have been varied and their effects on motility of the model cell tested in (Bottino 1996). For example, the membrane tension function (6) was replaced by a linear relation; the model cell with the Hookean membrane exhibited nearly 50% impaired motility and less volume retention that the standard cell with nonlinear membrane tension. Test runs involving nonlinear actin entanglements have not yet been implemented.

We now discuss several planned projects that will exploit the versatility and improve the biological accuracy of the model. A three-dimensional version of the cell model is currently being developed; the enhancements that follow are likely to be implemented first in the two-dimensional model before being adapted into the computationally intensive three-dimensional simulations.

The passive model cell will be used to investigate the effects of neutrophil viscoelasticity upon tumbling and adhesion on blood vessel walls and upon fluid flow and red block cell distribution in smaller arterioles and capillaries. An improvement on the model membrane already tested in Bottino (1997) will be to allow the membrane to slip tangentially to the membrane-embedded actin anchors. Due to the high diffusivity of membrane phospholipids, this "free-slip" behavior is thought to occur in ameboid cells.

In order to coordinate the active cytoskeletal events — in particular, actin polymerization, actomyosin contraction, and the establishment and relinquishment of transmembrane adhesions — future simulations will include an approximation of the reaction-advection-diffusion (RDA) equations modeling the signal transduction pathways thought to control ameboid cell movement. This will allow us to model chemoattractant diffusion, binding of chemoattractant to membrane receptors, internal signaling, and resultant polarization. We are developing techniques that will allow us to solve the RDA equations on the moving, deforming cell interior, and to interpolate the signal concentrations to the immersed boundary points. Links

among those points would exert appropriate protrusive or contractile forces based on the local signal concentrations.

Multiple copies of the model cell, each idependently traveling up a chemoattractant gradient, will be used to model the formation and movement of multicellular *Dictyostelium* slugs. A sufficiently general chemoattractant solver and simplified treatment of intracellular signaling will allow us to model the propagation of cAMP pulses from the initially starving cell to the entire population. This chemistry will be coupled with the mechanics of the formation of the cell aggregate and the traveling slug.

Acknowledgements The authors would like to thank Robert Dillon for his helpful suggestions during the course of this research, Hans Othmer for his careful reading of the manuscript, and Susan Jancart for prose optimization. The authors were supported in part by DOE Grant FG-01-93EW53023. The work of L. Fauci was supported in part by NSF Grant DMS-9501048.

References

Alberts B (1994) Molecular biology of the cell, 3rd edn. Garland, New York

Bottino DC (1996) An immersed boundary model of ameboid deformation and locomotion. Ph D thesis, Tulane University

Bottino DC (1997) Modeling viscoelastic networks in the context of the immersed boundary method (submitted for publication)

Bray D (1992) Cell movements. Garland, New York

Chien S (1984) Viscoelastic properties of leukocytes. In: Mieselman HJ, Lichtman MA, LaCelle PL (ed) White cell mechanics: basic science and clinical aspects. Liss, New York, pp 19–51

Cortese J (1989) Actin polymerization induces a shape change in actin-containing vesicles. Proc Natl Acad Sci USA 86:5773–5777

Devreotes PN, Zigmond SH (1988) Chemotaxis in eukaryotic cells: a focus on leukocytes and *dictyostelium*. Annu Rev Cell Biol 4:649–686

Dillon R, Fauci L, Gaver D (1995) A microscale model of bacterial swimming, chemotaxis and substrate transport. J Theor Biol 177:325–340

Evans EA (1984) Structural model for passive granulocyte behaviour based on mechanical deformation and recovery after deformation tests. In: Mieselman HJ, Lichtman MA, LaCelle PL (ed) White cell mechanics: basic science and clinical aspects. Liss, New York, pp 53–71

Fauci L, McDonald A (1995) Sperm motility in the presence of boundaries. Bull Math Biol 57:679–699

Fauci LJ (1990) Interaction of oscillating filaments: a computational study. J Comput Physics 86:294–313

Fauci LJ (1993) Computational modeling of the swimming of biflagellated algal cells. Contemp Math 141:91–102

Fauci LJ, Peskin CS (1988) A computational model of aquatic animal locomotion. J Comput Physics 77:85–108

Fogelson AL, Fauci LJ (1993) Truncated newton methods and the modeling of complex immersed elastic structures. Commun Pure Appl Math XSLVI:787–818

Fukui Y (1993) Toward a new concept of cell motility: cytoskeletal dynamics in ameboid movement and cell division. Int Rev Cytol 144:85–127

Janmey PA (1991) Mechanical properties of cytoskeletal polymers. Curr Opinion Cell Biol 2:4–11

Kroy K, Frey E (1996) Force-extension relation and plateau modulus for wormlike chains. Physical Rev Lett 77:306–309

Lackie J, Wilkinson P (1984) Adhesion and locomotion of neutrophil leukocytes on 2-d substrate and in 3-d matrices. In: White cell mechanics: basic science and clinical aspects. Liss, New York, pp 237–254

Oster G, Perelson A (1985) Cell spreading and motility: a model lamellipod. J Math Biol 21:383–388

Peskin C, McQueen D (1989a) A three-dimensional computational method for blood flow in the heart: I – immersed elastic fibers in a viscous incompressible fluid. J Comput Physics 81:372

Peskin C, McQueen D (1989b) A three-dimensional computational method for blood flow in the heart: II – contractile fibers. J Comput Physics 82:289

Peskin CS (1977) Numerical analysis of blood flow in the heart. J Comput Physics 25:220–252

Peskin CS, McQueen DM: A uniform finite difference grid navier-stokes solver (unpublished manuscript)

Sackmann E (1994) Intra- and extracellular macromolecular networks: Physics and biological function: Macromol Chem Phys 195:7–28

Schindl M, Walraff E, Deubzer B, Witke W, Gerisch G, Sackmann E (1995) Cell-substrate interactions and locomotion of *dictyostelium* wild-type and mutants defective in three cytoskeletal proteins: a study using quantitative reflection interference contrast microscopy. Biophys J 68:1177–1190

Tempel M, Isenberg G, Sackmann E (1996) Temperature-induced sol-gel transition and microgel formation in α-actinin cross-linked actin networks: a rheological study. Physical Rev E54: 1802–1810

Waugh R, Tsai M (1994) Shear rate-dependence of leukocyte cytoplasmic viscosity. In: Mieselman HJ, Lichtman MA, LaCelle PL (ed) Cell mechanics and cellular engineering. Springer, Berlin Heidelberg New York, pp 33–44

Wessels D, Soll D, Knecht D, Loomis W, De Lozanne A, Spudich J (1988) Cell motility and chemotaxis in *dictyostelium* amebae lacking myosin heavy chain. Develop Biol 128:164–177